INSTITUTE

FOR

AEROSPACE STUDIES

UNIVERSITY OF TORONTO

40 pages

IN-11165

SPECTRA OF NOISE AND AMPLIFIED TURBULENCE EMANATING FROM SHOCK-TURBULENCE INTERACTION: TWO SCENARIOS

by

Herbert S. Ribner

March 1986

UTIAS Technical Note No. 260
CN ISSN 0082-5263

SPECTRA OF NOISE AND AMPLIFIED TURBULENCE EMANATING FROM SHOCK-TURBULENCE INTERACTION: TWO SCENARIOS

by

Herbert S. Ribner

Submitted October, 1985

March 1986

UTIAS Technical Note No. 260
CN ISSN 0082-5263

UTIAS TECHNICAL NOTE NO. 260

ERRATA AND ADDENDA

Please replace pages 8 and 9 with the attached revised versions.

In the original page 9 the remarks concerning integration of dv_r and dv_ϕ were inadvertent and incorrect. Valid integrations apply only to the Cartesian forms du, dv, dw as set forth in Eq. (1a) of the new page 8. The components dv_r and dv_ϕ in cylindrical polars serve only to delineate the transfer functions of the shock-interaction process in simplest form. In the revision, the opportunity has been taken to expand page 8 by providing equations that, hopefully, clarify the verbal statements.

Page 5. Definitions of:

$\underline{K}$: In more conventional notation "θ" would be replaced by "$\theta + \pi/2$": see remarks below re definition of θ.

r, ϕ, X_1: Delete "of field point". [Refers to components of $\underline{K}$ and $d\underline{Z}$ describing shear wave (Figs. 1, 2).]

$\underline{X}$: Delete "or X_1, r, ϕ, Fig. 2)".

θ: θ is the polar angle of the velocity vectors, proportional to $d\underline{Z}$, in the shear wave, Fig. 1. The polar angle of the wavenumber vector $\underline{K}$, normal to this transverse wave, is $\theta + \pi/2$.

May 21, 1986

Acknowledgements

Support at the University of Toronto was aided by a grant from the Natural Sciences and Engineering Research Council of Canada and at the NASA Langley Research Center by tenure as a Distinguished Research Associate.

Abstract

This work is a small extension of our NACA studies of the early fifties that predicted amplification of turbulence on passing through a shock wave (observed for turbulent boundary layers), as well as the generation of intense noise (observed for supersonic jets). The first solved the basic gasdynamics problem of the interaction of an infinite planar shock with a single three-dimensional spectrum component of turbulence (an oblique sinusoidal "shear wave"). The second developed the comprehensive 3D spectrum analysis necessary to generalize the scenario to the interaction of a shock wave with convected homogeneous turbulence. Numerical calculations were carried out to yield curves (vs. Mach number) of rms sound pressure, temperature fluctuation, and two components of turbulent velocity downstream of the shock, for two cases of preshock turbulence. The present numerical study reproduces these for one case and provides in addition their one-dimensional power spectra (vs. wavenumber or frequency). Ratios of the several postshock spectra to the longitudinal preshock turbulence spectrum (1D) have been computed for a wide range of Mach numbers; curves vs. wavenumber are presented for two scenarios of preshock turbulence: isotropy and axisymmetry, both based on the von Karman 3D spectrum.

Contents

Nomenclature

$\tilde{a}$ = 1.3390, pure number

$\tilde{B}$ = $55/18\pi\tilde{a}$, pure number

c_A, c = pre- and postshock sound speeds, respectively

c^* = critical sound speed

I_{AC} = flux of acoustic energy from unit shock area

I_{TURB} = flux of preshock turbulence kinetic energy into unit shock area

$\underline{K}$ = nondimensional wavenumber vector (K_1, K_2, K_3 or K, θ, ϕ, Fig. 1; also K_r, K_1, θ, Fig. 2)

$\underline{k}$ = $K/\tilde{a}L$, actual wavenumber vector

L = longitudinal scale of turbulence

M_A = U_A/c_A, preshock Mach number

M_1 = U/c, postshock Mach number

P = transfer function relating dp'' to du

P = ambient pressure

p'' = pressure perturbation

T = transfer function relating $d\tau'$ to du

T = ambient temperature

r, ϕ, X_1 = cylindrical coordinates of field point

U_A, U = pre- and postshock stream velocity, respectively

u, v, w = nondimensional components of velocity perturbation in directions X_1, X_2, X_3, respectively (actual components/c^*)

$\underline{X}$ = nondimensional field point vector (X_1, X_2, X_3, Fig. 1, or X_1, r, ϕ, Fig. 2). X_1 is $\perp$ shock

$\underline{x}$ = $\underline{X}aL$, actual field point vector

$\tilde{X}$ = transfer function relating du' to du

$\tilde{Y}$ = transfer function relating dv_r' to dv_r

dZ_σ = (complex) wave amplitude associated with σ = u,r, ϕ, τ', p", etc.

γ = ratio of specific heats (taken as 1.4)

θ = polar angle (Figs. 1-3)

θ_{cr} = critical angle separating evanescent and nonevanescent pressure waves

ρ_A, ρ = fluid density upstream and downstream of shock, respectively

τ' = temperature perturbation

ϕ = azimuth angle (Figs, 1, 2)

Φ_σ = one-dimensional (1D) spectral density associated with σ = u, v, u', τ', p", etc.

ω = radian frequency ($2\pi \times$frequency)

Note: superscript ^ signifies actual dimensional quantity.

INTRODUCTION

Analytical studies of three-dimensional disturbances convected through — and interacting with — a shock wave seem to have commenced in the early 1950's.[1-4] The disturbances were waves of (1) vorticity, (2) entropy, or (3) sound; they were in the form of oblique planar, usually sinusoidal, patterns. Any one such wave encountering the shock would generate all three kinds on the downstream side. It was pointed out by Ribner[1,5,6] and by Batchelor[7] that the vorticity waves (called therein "shear waves") were three-dimensional Fourier components of arbitrary incompressible flows, e.g., weak turbulence. (See also Moyal.[8])

The initial papers[1-4] treated the interaction of individual waves of arbitrary inclination with an infinite plane shock; the analyses were linearized in terms of wave amplitude. A later paper[6] developed the comprehensive 3D spectrum analysis necessary to describe the interaction of turbulence with a shock; the earlier single-wave results were the "building blocks". Numerical calculations were carried out for rms values of turbulence velocity components, temperature, and pressure (sound) fluctuations downstream of the shock, assuming either isotropic or axisymmetric preshock turbulence. The plotted curves showed that velocity components of the post-shock turbulence would be amplified as much as 45% relative to preshock levels. Recent measurements do display the phenomenon of amplification (e.g., Refs. 9, 10).

The calculation of such turbulence amplification on passage through a shock has received renewed attention in recent years.[11-13] The term turbulence in this context is, however, a misnomer: these papers have reverted to dealing with a single 3D spectral component of turbulence. They oversimplify in interpreting the single-wave results as representative of the broad spectrum of waves constituting turbulence. On the other hand, two of them[12,13] pioneer in the application of numerical integration of the Euler equations to the single-wave shock-interaction problem. By coping with nonlinearity they test the range of applicability of the results of the linear analysis.

Some other studies based on the same fluid dynamics, but quite distinct in orientation, may be noted. These relate to the passage of a columnar vortex broadside through a planar shock wave: a cylindrical sound wave appears on the downstream side, partly cut off by the shock, as well as a modified vortex. The single-wave (single Fourier component) results of, e.g., Ref. 1, can serve as the "building blocks" to compute this sound wave in detail.[14,15] Unlike the shock-turbulence interaction problem, which is stochastic, this phenomenon is deterministic (and is more readily verifiable by experiment[16,17]). Nevertheless, the underlying analytical framework is the same. Both problems have been considered relevant to the generation of "shock noise" by turbulence passing through the shock pattern of a supersonic jet.[6,15,18]

It appears then that, despite other results both old and new, the only genuine calculations of turbulence interacting with a shock wave are those of the early reference 6. But these, as noted above, have been limited to rms values of the relevant disturbances: there are no computed spectra. The present study is an extension of that paper (in a very limited sense);

it seeks to provide the one-dimensional power spectra (vs. wave number or frequency) of velocity, temperature, and pressure perturbations, and of the acoustic energy flux emanating from the shock. The procedure is one of numerical integration of the corresponding 3D spectra. These are adapted from Ref. 6, with the 3D spectrum of the preshock turbulence specified.

SHOCK-TURBULENCE INTERACTION

Transfer Functions Connecting Fourier Components (Deterministic)

A snapshot of an arbitrary flow field may be represented by a Fourier-Stieltjes integral in three dimensions, as

$$u(\underline{X}) = \int du = \int dZ_u(\underline{K})\exp(i\underline{K}\cdot\underline{X}); \quad \underline{K} = K_1, K_2, K_3$$

$$v(\underline{X}) = \int dv = \int dZ_v(\underline{K})\exp(i\underline{K}\cdot\underline{X}); \quad |\underline{K}| \equiv K = 2\pi/\text{wavelength} \qquad (1a)$$

$$w(\underline{X}) = \int dw = \int dZ_w(\underline{K})\exp(i\underline{K}\cdot\underline{X}); \quad \underline{X} = X_1, X_2, X_3$$

This integral is effectively a superposition of plane sinusoidal waves with wavenumber $\underline{K}$ normal to the planes of constant phase; variation of $\underline{K}$ implies a distribution of wavelengths and orientations. We can apply this format to weak, essentially "frozen" turbulence (a pattern with negligible time dependence); this will behave almost incompressibly, governed by

$$\partial u/\partial X_1 + \partial v/\partial X_2 + \partial w/\partial X_3 \qquad (1b)$$

even though convected at high speed. Applying this constraint to (1a) shows that the amplitude $d\underline{Z}$ and wave number $\underline{K}$ are orthogonal:

$$K_1 dZ_u + K_2 dZ_v + K_3 dZ_w = \underline{K}\cdot d\underline{Z} = 0; \quad d\underline{Z} = dZ_u, dZ_v, dZ_w \qquad (1c)$$

Thus an individual wave is transverse; it may be interpreted physically as an oblique sinusoidal wave of shearing motion (Fig. 1).

Such a wave, when convected into a shock, interacts in a predictable fashion according to linear theory:[1-4] a "refracted" shear wave, a superposed entropy wave, and a pressure wave emerge on the downstream side. If the initial pattern of waves (upstream turbulence) is known only statistically, then the downstream pattern (modified turbulence, entropy "spottiness", and noise) can be determined statistically. That is, spectra, correlations, and mean square values can be calculated.

To this end, we incorporated the deterministic single-wave relations[1] into a comprehensive spectrum analysis in three dimensions[6] for homogeneous turbulence. A brief account of relevant parts of the development is given below. The physical quantities are normalized so as to be nondimensional:

u, v, w, etc. = velocity components/critical sound speed, c*
p" = pressure perturbation/ambient, $\hat{P}$
τ' = temperature perturbation/ambient, $\hat{T}$

(But addition of a superscript ^ to u, p", τ', etc., removes the normalization.)

It will be convenient to re-express the velocity field of an incident shear wave (Fig. 1) in cylindrical coordinates as (see also Fig. 2 where the wave is viewed edge-on)

$$\begin{aligned} du &= dZ_u \exp(i\,\underline{K}\cdot\underline{X}) \\ dv_r &= dZ_r \exp(i\,\underline{K}\cdot\underline{X}) \\ dv_\phi &= dZ_\phi \exp(i\,\underline{K}\cdot\underline{X}) \end{aligned} \tag{2}$$

where du is parallel to X_1 (normal to the shock), dv_r is parallel to r, and dv_ϕ is perpendicular to r and X_1 in the direction of increasing ϕ. The planes of constant phase $\underline{K}\cdot\underline{X}$ (= $\underline{k}\cdot\underline{x}$, see below) = constant make an angle θ with the X_1 axis. The wave number $\underline{K}$ and position vector $\underline{X}$ are non-dimensional; they are formed from their dimensional counterparts $\underline{k}$ and $\underline{x}$ as

$$\begin{aligned} \underline{K} &= \underline{k}\tilde{a}L; \quad L = \text{turbulence longitudinal scale} \\ \underline{X} &= \underline{x}/\tilde{a}L; \quad \tilde{a} = \text{pure number} \end{aligned} \tag{3}$$

respectively.

Figure 3 shows the results of the encounter of the incident wave, Eq. (2), with the shock. The three waves that appear on the downstream side are:

refracted shear wave, with components:

$$\begin{aligned} du' &= dZ'_u(\underline{K}')\exp(i\,\underline{K}'\cdot\underline{X}); \quad dZ'_u = \tilde{X}dZ_u \\ dv'_r &= dZ'_r(\underline{K}')\exp(i\,\underline{K}'\cdot\underline{X}); \quad dZ'_r = \tilde{Y}dZ_r \\ dv'_\phi &= dZ'_\phi(\underline{K}')\exp(i\,\underline{K}'\cdot\underline{X}); \quad dZ'_\phi = dZ_\phi \end{aligned} \tag{4}$$

entropy wave, aligned with refracted shear wave:

$$d\tau' = dZ'_\tau(\underline{K}')\exp(i\,\underline{K}'\cdot\underline{X}); \quad dZ'_\tau = TdZ_u \tag{5}$$

sound wave:

$$dp'' = dZ''_p(\underline{K}'')\exp(i\,\underline{K}''\cdot\underline{X}); \quad dZ''_p = PdZ_u \tag{6}$$

The planes of constant phase $\underline{K}'\cdot\underline{X}$ = constant and $\underline{K}''\cdot\underline{X}$ = constant make angles θ' and θ'', respectively, with the X_1 axis or shock normal (Fig. 3). These angles are functions of the angle θ of the incident wave (and of the Mach

number). For $|\theta|$ in the range from zero to a critical value θ_{cr}, the pressure wave decays exponentially with distance from the shock (in proportion to wave number): such waves are called evanescent. For $|\theta|$ in the range from θ_{cr} to $\pi/2$ the wave shows no decay and is called nonevanescent herein.

The right hand set of equations relates the respective amplitudes of the downstream waves with those of the initial shear wave components, dZ_u, dZ_r, dZ_ϕ. The transfer functions $\tilde{X}$, $\tilde{Y}$, T, and P are all dependent on the incident wave angle θ, as well as Mach number M; they are the results of a gasdynamic analysis carried out in Ref. 1. Functional expressions, taken or adapted therefrom, are given in Appendix A herein. The transfer functions are quite different in the regimes 0 to θ_{cr} and θ_{cr} to $\pi/2$; in particular, the form of P dictates evanescence in the former and nonevanescence in the latter.

Three-Dimensional and One-Dimensional Power Spectra (Stochastic)

For application to a stochastic field such as turbulence it is necessary to go over to statistical relations. If we form an ensemble average for waves of different wave numbers $\underline{K}$ and $\underline{\kappa}$ in respective ranges $d^3\underline{K}$ and $d^3\underline{\kappa}$ it is easily proved that

$$\overline{dZ_u(\underline{K})dZ_u^*(\underline{\kappa})} = [uu]\ \delta(\underline{\kappa} - \underline{K})d^3\underline{K}\ d^3\underline{\kappa}, \tag{7}$$

if the turbulence is homogeneous.[8,19] The quantity [uu] is a special symbol for the three-dimensional spectral density of $\overline{u^2}$ in wave number space $\underline{K}$. The vanishing of $\delta(\underline{\kappa}-\underline{K})$ for $\underline{\kappa} \neq \underline{K}$ implies that waves of different wavelengths or inclinations (since $\underline{\kappa}$ and $\underline{K}$ are vectors) are statistically independent.

The integral of (7) over $\underline{\kappa}$-space may be written, by virtue of the δ-function,

$$\overline{dZ_u(\underline{K})dZ_u^*(K)} = [uu]\ d^3\underline{K} \tag{8}$$

In similar fashion we can develop corresponding expressions for the 3D spectra [u'u'], [$\tau'\tau'$], [p"p"], etc. The integral of (8) over $\underline{K}$-space is $\overline{u^2}$, that of [$\tau'\tau'$] over K'-space is $\overline{\tau'^2}$, and so on.

Application of these procedures to (4) to (6) leads to[6]

$$\overline{u^2} = \iiint [uu] d^3\underline{K}$$

$$\overline{u'^2} = \iiint [u'u'] d^3\underline{K}' = \iiint |\tilde{X}|^2 [uu]\, d^3\underline{K} \tag{9}$$

$$\overline{\tau'^2} = \iiint [\tau'\tau'] d^3\underline{K}' = \iiint |T|^2 [uu] d^3\underline{K}$$

$$\overline{p''^2} = \iiint [p''p''] d^3\underline{K}'' = \iiint |P|^2 [uu] d^3\underline{K}$$

where the integration limits are $\pm \infty$ in K_1, K_2, K_3, etc.

We shall limit attention to axisymmetric turbulence, with main emphasis on the special case of isotropy. This and the axisymmetry of the shock interaction process led us in the earlier material[6] to employ cylindrical coordinates. In these coordinates,

$$d^3\underline{K} = d\phi\, K_r dK_r dK_1 \tag{10}$$

A first integration with respect to $d\phi$ then yields a factor 2π, so that

$$\overline{u^2} = 2\pi \int_{-\infty}^{\infty} \int_0^{\infty} [uu] K_r dK_r dK_1 \equiv \int_{-\infty}^{\infty} \Phi_u(K_1) dK_1$$

$$\overline{u'^2} = 2\pi \int_{-\infty}^{\infty} \int_0^{\infty} |\tilde{X}|^2 [uu] K_r dK_r dK_1 \equiv \int_{-\infty}^{\infty} \Phi_{u'}(K_1) dK_1 \tag{11}$$

$$\overline{\tau'^2} = 2\pi \int_{-\infty}^{\infty} \int_0^{\infty} |T|^2 [uu] K_r dK_r dK_1 \equiv \int_{-\infty}^{\infty} \Phi_{\tau'}(K_1) dK_1$$

$$\overline{p''^2} = 2\pi \int_{-\infty}^{\infty} \int_0^{\infty} |P|^2 [uu] K_r dK_r dK_1 \equiv \int_{-\infty}^{\infty} \Phi_{p''}(K_1) dK_1$$

respectively.

The last equality in each line defines a <u>one-dimensional</u> spectrum; these are explicitly:

$$\Phi_u(K_1) = 2\pi \int_0^\infty [uu]K_r dK_r$$

$$\Phi_{u'}(K_1) = 2\pi \int_0^\infty |\tilde{X}|^2[uu]K_r dK_r \qquad (12)$$

$$\Phi_{\tau'}(K_1) = 2\pi \int_0^\infty |T|^2[uu]K_r dK_r$$

$$\Phi_{p''}(K_1) = 2\pi \int_0^\infty |P|^2[uu]K_r dK_r$$

As formulated, all four spectra are functions of the upstream longitudinal wave number K_1. This is convenient and puts them on a common basis. Moreover, K_1 is proportional to radian frequency ω in the form

$$K_1 = \omega\tilde{a}L/U_A \qquad (13)$$

[This follows from

$$k_1 = \omega/U_A \qquad (14)$$

and the definition, Eq. (3), connecting the two k's.]

Although the interaction process of Fig. 3 conserves K_r but not K_1, ($K_1 \neq K_1' \neq K_1''$), the frequency ω is invariant ($\omega = \omega' = \omega''$). That is, an observer perceives the same frequency as each of the wave patterns moves past. This is, of course, a necessary result for a statistically steady process. A geometric analysis formally confirms the invariance of ω.

Isotropic Preshock Turbulence

For evaluation of the 1D spectra of (11) the 3D spectrum, [uu], of the input turbulence must be specified. The von Karman spectral model (called θ_{11} in Ref. 20) is chosen; in our notation it is

$$[uu] = \overline{u^2}\,\frac{\tilde{B}K_r^2}{2\pi[1 + K_1^2 + K_r^2]^{17/6}} \qquad (15)$$

$$\tilde{B} = 55/18\pi\tilde{a}, \qquad \tilde{a} = 1.3390$$

where the longitudinal scale L of the turbulence is incorporated in $K = k\tilde{a}L$. The pure number $\tilde{a}$ is a normalizing constant chosen so that

$$\int_{-\infty}^{\infty} dK_1 \int_0^{\infty} [uu] 2\pi K_r dK_r = \overline{u^2}$$

For numerical evaluation of the 1D spectra it will be convenient to express the cylindrical wave number component K_r in terms of the longitudinal component K_1 and the polar angle θ. This will replace the infinite range in K_r by a finite range in θ. It will also be easier to interpret the integral in terms of the geometry of Fig. 3. Compatibly with Ref. 6 (Eq. 56) we put (Figs. 1, 2):

$$K_1 = -K \sin\theta, \qquad K_2 = K \cos\theta \cos\phi$$

$$K_3 = K \cos\theta \sin\phi, \qquad K_r = \sqrt{K_2^2 + K_3^2} = |K_1| \cot\theta \tag{17}$$

$$dK_r = |K_1| \csc^2\theta d\theta$$

Inserting (15) and (17) into (11) gives, after some reduction, the following format for evaluation of the 1D spectra:

$$\frac{\Phi_i(K_1)}{\overline{u^2}} = \frac{\tilde{B}}{K_1^{5/3}} \int_0^{\pi/2} |\Gamma_i|^2 \frac{\cos^3\theta d\theta}{\sin^5\theta [b' + \cot^2\theta]^{17/6}} \tag{18}$$

where

$$b' = (1 + K_1^2)/K_1^2$$

and

$$\text{for } i = u,\ u',\ \tau',\ p'', \qquad \Gamma_i = 1,\ \tilde{X}\ T,\ P.$$

These express the general form to be numerically integrated for the shock-interaction products in the present case; namely, isotropic preshock turbulence with statistics described by the von Karman 3D spectrum.

One Dimensional Spectra of $\overline{v^2}$ and $\overline{v'^2}$

The one-dimensional spectra of $\overline{v^2}$ and $\overline{v'^2}$ involve a less straightforward derivation. The following section sets forth the basic equations and final spectra.

For isotropic and axisymmetric turbulence, $\overline{v^2} = \overline{w^2}$ upstream of the shock and $\overline{v'^2} = \overline{w'^2}$ downstream of the shock: the respective 1D spectra have similar equalities. The corresponding 3D spectra, [vv] and [ww], [v'v'] and

[w'w'], are not respectively equal, nor are they axisymmetric. The sums, however, can be shown to be axisymmetric: they depend on K_r rather than on K_2 and K_3 separately. These sums on both sides of the shock have a relatively simple connection,[6]

$$[v'v'] + [w'w'] = (|\Upsilon|^2 - 1)\tan^2\theta\,[uu] + [vv] + [ww], \qquad (19)$$

where the analytical form of the transfer function Υ is given in Appendix A herein.

We now restrict ourselves to the special case of isotropic preshock turbulence. Then invoking the cited equalities and the axisymmetry of (19) and employing the input spectrum and methods of the last section leads to the desired 1D-spectra (details are given in Appendix B). The results are:

$$\frac{\Phi_V(K_1)}{\overline{u^2}} = \frac{B}{2K_1^{5/3}} \int_0^{\pi/2} \frac{(2 + \cot^2\theta)\cos\theta\, d\theta}{\sin^3\theta[b' + \cot^2\theta]^{17/6}} = \frac{\Phi_W(K_1)}{\overline{u^2}} \qquad (20)$$

$$\frac{\Phi_{V'}(K_1)}{\overline{u^2}} = \frac{\Phi_V(K_1)}{\overline{u^2}} + \frac{B}{2K_1^{5/3}} \int_0^{\pi/2} \frac{(|\tilde{\Upsilon}|^2 - 1)\cos\theta\, d\theta}{\sin^3\theta[b' + \cot^2\theta]^{17/6}} = \frac{\Phi_{W'}(K_1)}{\overline{u^2}} \qquad (21)$$

One-Dimensional Spectrum of Acoustic Energy Flux

The last of equations (18) gives the 1D spectrum of the sound pressure generated downstream by the passage of isotropic turbulence through a shock. The connection to acoustic energy flux is not trivial, as in the case of quasi-plane waves propagating through still air. An analysis has been given by Ribner[21] invoking energy flow relations for a moving medium (Blokhintsev[22]). The integral of Eq. (15) of Ref. 21 reads, in the present notation,

$$\hat{I}_{AC} = \frac{\hat{p}^2}{\rho c} \int_{\theta_{cr}}^{\pi/2} \overline{dp''^2}(\theta'')(1 + M_1\sin\theta'')(M_1 + \sin\theta'') \qquad (22)$$

This evaluates the flux of acoustic energy emanating from unit area of the shock. Since only nonevanescent waves figure in I_{AC}, the limits of integration correspond to that range. The result after numerical integration is plotted in Ref. 21.

The quantity $\overline{dp''^2}(\theta)$ can be identified with the integrand (including the 2π factor) of the last of Eqs. (11) herein. Hence the further development leading to the last of Eqs. (18) may be applied. This yields the one-dimensional spectrum of this flux, $\hat{\Phi}_{AC}(K_1)$, in the form

$$\frac{\hat{\Phi}_{AC}(K_1)}{\hat{I}_{TURB}} = \frac{2}{5\gamma^2}\left(\frac{c}{c^*}\right)^2 \frac{\hat{B}}{M_1 K_1^{5/3}} \int_{\theta_{cr}}^{\pi/2} \frac{|P|^2(1 + M_1\sin\theta'')(M_1 + \sin\theta'')\cos^3\theta d\theta}{\sin^5\theta\,[b' + \cot^2\theta]^{17/6}}, \tag{23}$$

when the input turbulence has the von Karman (3D) spectrum. This flux has been ratioed to the flux of kinetic energy of turbulence through the shock,

$$\hat{I}_{TURB} = \frac{5}{2}\rho_A U_A c^{*2}\,\overline{u^2} = \frac{5}{2}\rho U c^{*2}\,\overline{u^2} \tag{24}$$

(The — perhaps surprising — factor 5/2 results from the definition

$$\hat{I}_{TURB} = \frac{1}{2}\rho_A\,\overline{[(U_A + c^*u)^2 + (c^*v)^2 + (c^*w)^2](U_A + c^*u)} - \frac{1}{2}\rho_A U_A^3 \tag{25}$$

and the postulated isotropy, $\overline{u^2} = \overline{v^2} = \overline{w^2}$.)

One-Dimensional Spectral Ratios; Lack of Uniqueness (Aliasing)

The component of turbulent velocity normal to the shock — called u herein — has a central role in the analysis. The three dimensional spectrum of $\overline{u^2}$ governs the shock-interaction effects, and the resulting 1D spectra are conveniently scaled to $\overline{u^2}$. Suppose, however, that we scale these 1D spectra to the 1D spectrum of $\overline{u^2}$: then this ratio in each case may be regarded as a sort of power spectrum transfer function; it will be a function of K_1. Up to this point these quantities have been evaluated only for the von Karman 3D preshock spectrum, a particular case of isotropic turbulence. The question may now be asked, how much will these spectral ratios change with changes in the preshock spectrum?

Such changes will be explored in the present section. They are expected to be nonzero because the 1D spectrum of $\overline{u^2}$ (in K_1) does not uniquely determine its 3D spectrum (in K_1, K_2, K_3) on which the shock interaction depends. (The 3D spectrum, on the other hand, does uniquely determine the 1D spectrum as a result of the double integration over K_2 and K_3.) This lack of uniqueness has been termed an aliasing effect. We shall apply the term as well to lack of uniqueness in the postshock/preshock 1D spectral ratios.

A geometric interpretation may be developed with the aid of Fig. 2. The 3D spectrum of turbulence is an aggregate of waves like the one shown with a wide range of wavelengths $2\pi/K$ and angles θ (and ϕ). If $\Phi(K_1)$ is the 1D spectrum, the differential $\Phi(K_1)dK_1$ is a narrow band of these waves with component wavelengths close to $2\pi/K_1$. It is evident that a variety of wave inclinations θ with appropriate wavelengths $2\pi/K$ (functions of θ) could be

chosen to have this same x_1-direction intercept $2\pi/K_1$. Thus the 3D wave pattern corresponding to $\Phi(K_1)$ is not unique.

Axisymmetric Turbulence

A convenient example of aliasing changes in spectral ratios can be obtained by modifying the preshock spectrum to change it from full isotropy ($\overline{v^2} = \overline{w^2} = \overline{u^2}$) to axial symmetry ($\overline{v^2} = \overline{w^2} \neq \overline{u^2}$). The conditions for a 3D spectrum tensor to be axisymmetric have been discussed by Batchelor[23] and others; for full generality they are very complex. However, we are concerned here with but an example of axisymmetry. This can be obtained from the von Karman spectrum (a particular case of isotropic turbulence) by a simple modification: we merely multiply the longitudinal spectrum [uu] (the only one of concern herein) by an arbitrary non-negative function of wave angle θ (or of $K_1/K_r = \tan\theta$). (θ is considered to be a polar angle and is restricted to the range 0 to $\pi/2$.)

This axisymmetric spectrum then takes the form

$$[uu]_{AXI} = F^2(\theta)\,[uu] \tag{26}$$

This is justified by comparison with the second of Eqs. (12)

$$[u'u'] = |\tilde{X}|^2\,[uu] \tag{27}$$

that relates the postshock longitudinal spectrum, [u'u'], to the preshock value, [uu], $\tilde{X}$ being the transfer function. There being no preferred direction in the plane of the shock ($\perp$ to u), [u'u'] must surely be axisymmetric. But the argument for axisymmetry does not depend on the particular form of the factor X: it could be an arbitrary function of K_1/K_r (or of θ).

For our particular example we shall take

$$[uu]_{AXI} = [uu]\cos^N\theta, \qquad \text{with } N = 2 \tag{28}$$

to describe the 3D axisymmetric preshock longitudinal spectrum in terms of an isotropic form [uu]; specifically, the latter is taken as the von Karman form that we have used throughout. For this case the 1D spectra $\Phi_{\mu}(K_1)$, $\Phi_{u'}(K_1)$, $\Phi_{\tau'}(K_1)$, and $\Phi_{p''}(K_1)$ are given by Eqs. (12) with an extra factor $\cos^2\theta$ in the integrands.

RESULTS AND DISCUSSION

Isotropic Preshock Turbulence

RMS Values of Postshock Disturbances, and Noise in Decibels

Figure 4 gives the variation with upstream Mach number of the various shock interaction products for a specific scenario: the preshock turbulence is isotropic with an intensity of 1% of free stream. The curves display rms perturbations of longitudinal velocity u and lateral velocity v or w in percent of initial stream velocity, and of rms temperature and pressure (noise) in percent of ambient. The figure is adapted from Fig. 4 of Ref. 6. The curves represent, in effect, the integrals with respect to K_1 of the respective one-dimensional spectra; that is, the integrals displayed in Eqs. (11). (The actual procedure, however, bypassed the 1D spectra and employed only the specification of preshock isotropy. The results are independent of the preshock spectra, 3D or 1D, so long as they are consistent with isotropy.)

The amplification of both the longitudinal and lateral components of the postshock turbulence is evident; it reaches some 45%, as noted in the Introduction, for the lateral component at high Mach number. The other two curves in Fig. 4 refer to the temperature and pressure fluctuations, respectively. (These are both spatial and temporal: rms values are the same from either point of view.) In first order, these are absent from the postulated upstream flows (extremely weak second order pressure and isentropic temperature fluctuations are associated with the specified 1% preshock turbulence).

On an acoustical basis the pressure fluctuation (noise) generated by the shock-turbulence interaction is very intense. This is shown in Fig. 5, where the noise level in decibels corresponding to Fig. 4 is plotted vs. Mach number. (The definition is

$$dB = 20 \log_{10}(\sqrt{\overline{p''^2}}/\tilde{P}_{REF}); \qquad \tilde{P}_{REF} = 2\times10^{-10} \text{ atm} \tag{29}$$

when the postshock ambient pressure is taken as 1 atmosphere.) For 1% preshock turbulence the postshock noise level is predicted to exceed 140 dB for all upstream Mach numbers above 1.05.

Figure 6 displays normalized (nondimensional) 1D power spectra calculated from the equations presented herein; the scenario is isotropic turbulence, governed by the von Karman 3D spectrum, being convected by an M = 1.25 flow into a normal shock. The six spectra are:

$\hat{\Phi}_u(K_1)/\overline{\hat{u}^2}$ longitudinal comonent of preshock turbulence

$\hat{\Phi}_{u'}(K_1)/\overline{\hat{u}^2}$ longitudinal component of postshock turbulence

$\hat{\Phi}_{\tau'}(K_1)/\hat{T}^2$	temperature fluctuation
$[\hat{\Phi}_{p''}(K_1)/\hat{P}^2]_{X=0}$	pressure fluctuation just downstream of shock (acoustic near field)
$[\hat{\Phi}_{p''}(K_1)/\hat{P}^2]_{X=\infty}$	pressure fluctuation far downstream of shock (acoustic far field)
$\hat{\Phi}_{AC}(K_1)/\hat{I}_{TURB}$	acoustic energy flux emanating from shock

The first two of these are normalized by $\overline{u^2}$, which is the integral (from $-\infty$ to ∞ in K_1) of $\Phi_u(K_1)$ (thus the integral of the first is unity). The next three are normalized by one or the other of (ambient temperature)^2 and (ambient pressure)^2. Finally, $\hat{\Phi}_{AC}$ is normalized by the flux of kinetic energy of preshock turbulence flowing into the shock. The superscript signifies a dimensional value, unsuperscripted forms having been nondimensionalized at the outset of the analysis.

The pressure field (noise) decays from an extremely high value just downstream of the shock (X=0) to an asymptotic lower value — still very intense acoustically — far downstream (X=∞). Figure 6 shows a major difference in their spectral content: the X-0 near field is dominated by low frequencies, decaying asymptotically like $K_1^{-5/3}$ beyond $K_1 \equiv 3$. The X=∞ far field is very deficient in low frequencies; on a linear scale it has a bell-shaped spectrum, peaking near $K_1=1$, but with the same asymptotic decay (the Kolmogorov $K_1^{-5/3}$ law) beyond $K_1 \cong 3$.

One-Dimensional Spectra and Postshock/Preshock Spectral Ratios

Figure 6 applies for M=1.25; a series of such figures could be presented for a wide range of Mach numbers. A much neater alternative, however, is to ratio each of these spectra at each value of K_1 to the $\Phi_u/\overline{u^2}$ spectrum. This ratio, as has been mentioned earlier, could be regarded as a sort of transfer function connecting the ratioed pair of spectra. In this format the variation with Mach number can be discerned much more systematically.

Figure 7 presents such spectral ratios: it relates the postshock to the preshock longitudinal component of turbulence (the $\overline{u^2}$ divisors cancel) for a series of Mach numbers, M. For convenience the curves are normalized by factors Z(M) (tabulated on the figure) to force agreement with the M=1.25 curve at $K_1=1$; this makes the family of curves much more compact. It is seen that increasing Mach number enhances the low frequencies of the longitudinal component of the postshock turbulence.

Figure 8 gives the corresponding spectral ratios relating postshock lateral component of turbulence to preshock longitudinal component. Here the behaviour is the reverse of that in Fig. 7: increasing Mach number for the most part decreases the low frequency content.

Figure 9 gives the spectral ratios relating postshock temperature fluctuation (arising from entropy "spottiness" generated at the shock) to preshock longitudinal component of turbulence. It is evident that the low frequencies in the temperature field are somewhat enhanced compared with those of the turbulence field. The variation is not, however, monotonic with Mach number: there is a foldover of the curves with increasing M.

Figures 10 and 11 give the spectral ratios relating the near field and far field pressure fluctuations (noise), respectively, to the longitudinal component of the preshock turbulence. The two families of curves are clearly very different. Moving on, Fig. 12 displays the spectral ratios connecting the acoustic energy flux emitted by the shock on the downstream side to, again, the longitudinal component of preshock turbulence. One notes the marked qualitative similarity with Fig. 11. This is not surprising, since acoustic energy flux and far-field mean square pressure fluctuation are closely related. For a medium at rest the two are exactly proportional, whereas in the postshock flow they differ as described by Blokhintsev[22] for a moving medium.

Axisymmetric Preshock Turbulence

Postshock/Preshock Spectral Ratios; Aliasing Effect

Calculations parallel to some of those pertaining to Figs. 7 to 12 (isotropic turbulence, von Karman spectrum) have been carried out for a specified axisymmetric preshock turbulence. As described in the relevant earlier section, the two 3D preshock longitudinal spectra are related by Eq. (28).

Figure 13 gives the 1D spectral ratio of postshock to preshock longitudinal component of turbulence for the axisymmetric preshock turbulence specdified above, when [uu] is the von Karman spectrum (see, e.g., Ref. 20). Also plotted is the 1D spectrum $\Phi_u/\overline{u^2}$ of the longitudinal component of the preshock turbulence. (Normalization of Φ_u is by the same $\overline{u^2}$ as for Figs. 7-12, not by $\overline{u^2}_{AXI}$.) Comparison with Fig. 6 (isotropic turbulence) shows that the two spectra of $\Phi_u/\overline{u^2}$ are vastly different. Nevertheless, the spectral ratios of Fig. 7 (isotropic turbulence) and Fig. 13 (axisymmetric turbulence) are qualitatively rather similar, although quantitatively different. The spectral ratios are, in fact, very much less dissimilar than the spectra of the two kinds of turbulence. This property points up the utility of the 1D spectral ratio in describing shock-turbulence interaction effects.

The fact that the spectral ratios do change (although not radically) with marked changes in the 3D spectrum of the preshock turbulence is a consequence of the aliasing effect discussed earlier. Comparison of Figs. 7 and 13 gives a measure, for a particular pair of cases, of this aliasing effect.

Figure 14 gives the spectral ratio relating postshock temperature fluctuation to preshock longitudinal component of turbulence. This figure (axisymmetric preshock turbulence) is to be compared with Fig. 9 (isotropic

turbulence). Again, the sets of spectral ratios are qualitatively generally similar. The differences (aliasing effect) are greater than those between Figs. 7 and 13.

Finally, Fig. 15 gives the spectral ratio relating the far field ($X=\infty$) pressure fluctuations (noise) to the longitudinal component of preshock turbulence. This figure (axisymmetric preshock turbulence) is to be compared with Fig. 11 (isotropic preshock turbulence). The same sort of qualitative similarity is found between Figs. 9 and 14. The first glance impression of the similarity is, however, a bit misleading, e.g., for $K \leq 1$ it is the $M=1.01$ curve of Fig. 11 that is very similar to the $M=1.05$ curve of Fig. 15.

These three figures, taken together, give some idea of the changes in spectral ratio (the aliasing effect) due to changes in the 3D spectrum of the preshock turbulence. But this one comparative example of axisymmetric vs. isotropic turbulence hardly quantifies the effect.

APPENDIX A

GENERAL RELATIONS AND TRANSFER FUNCTIONS

The upstream Mach number M and the incident wave inclination θ (Figs. 1-3) are specified. These dictate a virtual Mach number $\bar{W}$. A number of general relations are independent of the magnitude of $\bar{W}$; the remainder, notably the transfer functions, take different functional forms, depending on whether $\bar{W}<1$ or >1. The ratio of specific heats γ is taken as 1.4. (For formulas in terms of γ see Ref. 6.)

General Relations

M = specified

$m = 6M^2/(M^2+5)$

$M_1 = \sqrt{(M^2+5)/(7M^2-1)}$

θ = specified

$\theta' = \tan^{-1}(m\tan\theta)$

$\bar{W} = M_1/\cos\theta'$

$\beta^2 = 1-M^2$

$\beta_W = \sqrt{|1-\bar{W}^2|}$

$\mu = \tan^{-1}(1/\beta_W)$

$\theta'_{cr} = \cos^{-1}M_1$

$\theta_{cr} = \cot^{-1}(m\cot\theta'_{cr})$

$\theta''_{cr} = \theta'_{cr} - \pi/2$

$\theta'' = -\tan^{-1}\left[\frac{M_1^2\tan\theta'}{\beta^2}\right]$ for $\bar{W} \leq 1$

$= \theta' - \mu$ for $\bar{W} \geq 1$

Transfer Functions

These are defined in terms of functions of other functions. For numerical calculation the sequence should be in reverse order to the listing. The relative ease of programming belies an appearance of complexity.

$W \leq 1$ $(0 \leq \lvert\theta\rvert \leq \theta_{cr}$		$W \geq 1$ $(\theta_{cr} \leq \lvert\theta\rvert \leq \pi/2$	
P	$= -\dfrac{2.8\Pi\sqrt{m}}{(2.4m-.4)\cos\theta\cos\theta'} e^{i\delta_p}$	P	= No Change
Π	$= \dfrac{(\cos\theta)}{m}\dfrac{\sqrt{c^2+d^2}}{\beta} e^{-K_r X \beta_\omega'/\beta^2}$	Π	$= \dfrac{\cos\theta\sin\mu}{m\cos\theta''} c$
T	$= \sqrt{(a\tan\theta-1)^2 + (b\tan\theta)^2}$ $*0.8(m-1)^2/[2.4m-.4)\sqrt{m}] e^{i\delta_T}$	T	= N.C., with b = 0
δ_s	$= \tan^{-1}(-B/A)$	δ_s	= 0
δ_T	$= \tan^{-1}[b/(\cot\theta-a)]$	δ_T	= 0
δ_p	$= \tan^{-1}\dfrac{c\beta_w - d\tan\theta'}{d\beta_w + c\tan\theta'}$	δ_p	= 0
$\tilde{X}$	$= [S\cos\theta'/\cos\theta]e^{i\delta_S}$	$\tilde{X}$	= N.C.
$\tilde{Y}$	$= [S\sin\theta'/\sin\theta]e^{i\delta_S}$	$\tilde{Y}$	= N.C.
S	$= (\sqrt{A^2 + B^2}/m)\cos\theta$	S	= N.C., with B = 0
A	$= \sec\theta' + 2(m-1)\cos\theta' + (a/m)(m-1)^2\sin\theta'$	A	= N.C.
B	$= (b/m)(m-1)^2\sin\theta'$	B	= 0
c	$= D'a/m - F'$	c	= N.C.
d	$= D'b/m$	d	= 0
a/m	$= (CE + DF)/(C^2 + D^2)$	a/m	$= (C' + GF')/(E' + GD')$
b/m	$= (CF - DE)/(C^2 + D^2)$	b/m	= 0
C	$= (1/6 + 2m/3)\tan\theta' -(1/2)[(m-1)^2+(m-1)/1.2]\sin2\theta'$	C'	$= m/3 - 2[1 + (m-1)\cos^2\theta']$
D	$= D'\beta_w/\beta^2$	D	= Not used
D'	$= (m-1)[1 + (m-1)\cos^2\theta']$	D'	= N.C.
E	$= 2 - m/3 + 2(m-1)(\beta_w^2/\beta^2)\cos^2\theta'$	E'	$= F'(m-1)/2 - (1+2m/3)\tan\theta'$

F	$= F'\beta_w/\beta^2$	F	= Not used
F'	$= (m-1)\sin 2\theta'$	F'	= N.C.
G	= Not used	G	$= -\tan\theta''$

Note: Errors have been found in one or the other of the two versions of Ref. 6 from which the above are taken or derived; these occur in several equations and in the list of symbols. Those that are applicable have been corrected. Some other errata are corrected in Appendix D herein.

APPENDIX B

ONE-DIMENSIONAL SPECTRA OF $\overline{v^2}$ AND $\overline{v'^2}$

The starting point is Eq. (19):

$$\{[v'v'] + [w'w']\}d^3\underline{K} = (|\tilde{Y}|^2 - 1)\,[uu]\tan^2\theta\, d^3\underline{K} + \{[vv] + [ww]\}d^3\underline{K}$$

Invoking the axisymmetry, we may integrate as in Eqs. (11) and (12):

$$2\pi\int_o^\infty\{v'v'] + [w'w']\}k_r dK_r = 2\pi\int_o^\infty(|\tilde{Y}|^2-1)\,[uu]\tan^2\theta\, K_r dK_r + 2\pi\int_o^\infty\{[vv] + [ww]\}K_r dK_r \qquad (B1)$$

The left-hand side is the sum of $\Phi_{v'}(K_1)$ and $\Phi_{w'}(K_1)$; they are equal, even though their respective integrands are not. This implies

$$2\Phi_{v'}(K_1) = 2\Phi_{w'}(K_1) = 2\pi\int_o^\infty(|\tilde{Y}|^2-1)\,[uu]\tan^2\theta\, K_r dK_r + 2\pi\int_o^\infty\{[vv] + [ww]\}\,K_r dK_r \qquad (B2)$$

Applying the same argument to the right-hand side shows that the second integral may be interpreted as $2\Phi_v(K_1) = 2\Phi_w(K_1)$.

Isotropic Turbulence

If we designate u, v, w as q_1, q_2, q_3, then the general spectral form for isotropic turbulence is:[7]

$$[q_i q_j] = \frac{E(K)}{4\pi K^4} (K^2 \delta_{ij} - K_i K_j) \tag{B3}$$

We take $E(K)/4\pi K^4$ to have the von Karman form

$$\frac{E(K)}{4\pi K^4} = \frac{\tilde{B}\,\overline{u^2}}{2\pi} \frac{1}{[1+K^2]^{17/6}} \tag{B4}$$

Then, after a little manipulation,

$$[uu] = \frac{\tilde{B}\,\overline{u^2}}{2\pi} \frac{K_r^2}{[1+K_1^2+K_r^2]^{17/6}} \tag{B5}$$

$$[vv] + [ww] = \frac{\tilde{B}\,\overline{u^2}}{2\pi} \frac{2K_1^2 + K_r^2}{[1+K_1^2+K_r^2]^{17/6}} \tag{B6}$$

where $K_r^2 = K_2^2 + K_3^2$. Insertion into (B2) then yields

$$\Phi_v(K_1) = \Phi_w(K_1) = \frac{\tilde{B}\,\overline{u^2}}{2} \int_0^\infty \frac{(2K_1^2+K_r^2)K_r dK_r}{[1+K_1^2+K_r^2]^{17/6}} \tag{B7}$$

$$\Phi_{v'}(K_1) = \Phi_{w'}(K_1) = \Phi_v(K_1)$$

$$+ \frac{\tilde{B}\,\overline{u^2}}{2} \int_0^\infty \frac{(|\tilde{Y}|^2-1)K_r^2(\tan^2\theta)K_r dK_r}{[1+K_1^2+K_r^2]^{17/6}} \tag{B8}$$

Invoking polar coordinates in the form of Eq. (17) yields:

$$\Phi_v(K_1) = \Phi_w(K_1) = \frac{\tilde{B}\,\overline{u^2}}{2K_1^{5/3}} \int_0^{\pi/2} \frac{(2+\cot^2\theta)\cos\theta\, d\theta}{\sin^3\theta[b'+\cot^2\theta]^{17/6}} \qquad (B9)$$

$$\Phi_{v'}(K_1) = \Phi_{w'}(K_1) = \Phi_v(K_1) +$$

$$\frac{\tilde{B}\,\overline{u^2}}{2K_1^{5/3}} \int_0^{\pi/2} \frac{(|\tilde{Y}|^2-1)\cos\theta\, d\theta}{\sin^3\theta[b'+\cot^2\theta]^{17/6}} \qquad (B10)$$

where $b' = (1+K_1^2)/K_1^2$, and $\tilde{Y}$ is defined in Appendix A. Equations (B9) and (B10) are the desired one dimensional integrals [cited as (20) and (21), respectively, in the main text].

APPENDIX C

OBLIQUE SHOCKS

The analysis and results, on a wavenumber basis, may be applied to oblique shocks by the usual procedure. The equivalent normal shock transformation

$$M = M_0\cos\phi \quad \text{or} \quad U_A = U_0\cos\phi \qquad (C1)$$

is made, where M_0 is the upstream Mach number, and ϕ is the oblique angle between the shock normal and the upstream flow direction. In Figs. 4 and 5, the designation "1% preshock turbulence" is now to be interpreted as "($\cos\phi$)% preshock turbulence".

The interpretation of all figures in terms of wavenumber K_1 is unaltered, except for Fig. 12 (acoustic energy flux). That figure is inapplicable to oblique shocks: the structure of the underlying equations (22) and (23) is changed, and no simple proportionality will serve.

The proportionality of K_1 to frequency, however, does not carry over to the oblique shock case:* equations (13) and (14) are inapplicable. If $\tilde{K}_1$ is the component wavenumber along the stream velocity U_0, then the two equations are replaced by

*An exception is the case of $\Phi_u(K_1)$ for isotropic preshock turbulence.

$$\tilde{K}_1 = \omega\tilde{a}L/U_0 \tag{C2}$$

and

$$\tilde{k}_1 = \omega/U_0 \tag{C3}$$

respectively. Thus $\tilde{K}_1$ takes over the role of K_1 (and U_0 the role of U_A).

It follows that 1D spectra in terms of $\tilde{K}_1$, rather than K_1, are equivalent to frequency spectra in the oblique shock case. This implies a coordinate axis rotation of amount ϕ about the OX_3 axis:

$$\begin{aligned}\tilde{K}_1 &= K_1\cos\phi + K_2\sin\phi \\ \tilde{K}_2 &= -K_1\sin\phi + K_2\cos\phi \\ \tilde{K}_3 &= K_3\end{aligned} \tag{C5}$$

with inverse

$$\begin{aligned}K_1 &= \tilde{K}_1\cos\phi - \tilde{K}_2\sin\phi \\ K_2 &= \tilde{K}_1\sin\phi + \tilde{K}_2\cos\phi \\ K_3 &= \tilde{K}_3\end{aligned} \tag{C6}$$

Also spherical polar and cylindrical coordinates are defined about the $\tilde{K}_1$-axis, similar to (17); thus (since the magnitude $\tilde{K} = K$),

$$\tilde{K}_1 = -K\sin\tilde{\theta}, \qquad \tilde{K}_2 = K\cos\tilde{\theta}\cos\tilde{\phi}$$

$$\tilde{K}_3 = K\cos\tilde{\theta}\sin\tilde{\phi} \qquad \tilde{K}_r = \sqrt{\tilde{K}_2^2 + \tilde{K}_3^2} = |\tilde{K}_1|\cot\tilde{\theta} \tag{C7}$$

$$d\tilde{K}_r = |\tilde{K}_1|\csc^2\tilde{\theta}\,d\tilde{\theta}$$

In order to obtain the various 1D spectra in terms of $\tilde{K}_1$ rather than K_1, Eq. (12) must be rewritten with $\tilde{K}_r$ and (implicitly) $\tilde{\phi}$, $\tilde{\theta}$ replacing K_r,

ϕ, θ, respectively. Also the factor 2π must be replaced by an integration over $d\tilde{\phi}$; this is required since the transfer functions $|\Gamma_i|$ depend on both $\tilde{\phi}$ and $\tilde{\theta}$, not $\tilde{\theta}$ alone. Stated otherwise, the $|\Gamma_i|$ are axisymmetric relative to the shock normal direction (along which K_1 is measured), but not axisymmetric relative to the oblique-shock flow direction (along which $\tilde{K}_1$ is measured). The 1D spectra are thus

$$\Phi_i(\tilde{K}_1) = \int_0^{2\pi} d\tilde{\phi} \int_0^{\infty} |\Gamma_i|^2 [uu] \tilde{K}_r d\tilde{K}_r \tag{C8}$$

Because of the postulated isotropy of the preshock turbulence, [uu] has the same form in the rotated reference frame as in the original frame. Thus it takes the form (15), but with $\tilde{K}_1$, $\tilde{K}_r$ replacing K_1, K_r respectively. Then, with the use of Eqs. (C6) and (C7), the explicit form of the 1D spectra is

$$\frac{\Phi_i(\tilde{K}_1)}{\overline{u^2}} = \frac{\tilde{B}}{\tilde{K}_1^{5/3}} \int_0^{2\pi} \frac{d\tilde{\phi}}{2\pi} \int_0^{\pi/2} |\Gamma_i|^2 \frac{\cos^3\tilde{\theta} d\tilde{\theta}}{\sin^5\tilde{\theta}[\tilde{b}' + \cot^2\tilde{\theta}]^{17/6}} \tag{C9}$$

where $|\Gamma_i| = |\Gamma_i|(\theta)$ is defined in Eq. (18), $b' = (1 + \tilde{K}_1^2)/\tilde{K}_1^2$, and the angle θ is evaluated from

$$\begin{aligned} \theta &= \tan^{-1}(|K_1|/\sqrt{K_2^2 + K_3^2}) \\ &= \tan^{-1} \frac{|\cos\psi - (\tilde{K}_2/\tilde{K}_1)\sin\psi|}{[\sin^2\psi + (\tilde{K}_2/\tilde{K}_1)^2\cos^2\psi + (\tilde{K}_2/\tilde{K}_1)\sin 2\psi + (\tilde{K}_3/\tilde{K}_1)^2]^{1/2}} \end{aligned} \tag{C10}$$

with

$$\begin{aligned} \tilde{K}_2/\tilde{K}_1 &= -\cot\tilde{\theta}\cos\tilde{\phi} \\ K_3/K_1 &= -\cot\tilde{\theta}\sin\tilde{\phi} \end{aligned} \tag{C11}$$

Equation (C9), with (C10) and (C11), evaluates the 1D spectra in the form of a double integral. Thus two numerical quadratures are required (in $\tilde{\phi}$ and $\tilde{\theta}$) for the oblique shock case. By contrast, only a single numerical quadrature was required (in θ) for the normal shock case.

APPENDIX D

CORRECTIONS TO THE BASIC REFERENCE, RIBNER (1954)[6]

The corrected equations are:

$$\overline{v'^2} + \overline{w'^2} = \int \frac{|S|^2 \sin^2\theta' - \sin^2\theta}{\cos^2\theta} [uu]\, d\underline{k} + \overline{v^2} + \overline{w^2} \tag{54}$$

$$[uu] = k^{-2} F(k) \cos^2\theta \tag{55}$$

$$\overline{u^2} = 2 \int_0^\infty F(k)dk \int_0^{2\pi} d\phi \int_0^{\pi/2} \cos^3\theta d\theta \tag{57}$$

$$\overline{u'^2} = 2 \int_0^\infty F(k)dk \int_0^{2\pi} d\phi \int_0^{\pi/2} |S|^2 \cos^2\theta' \cos\theta d\theta \tag{58}$$

Corrections to the definitions in Table A (Symbols) are:

T	Multiply by -1
θ''	$= -\tan^{-1} \frac{M_1^2 \tan\theta'}{1-M_1^2}, \quad 0 \leq \theta \leq \theta_{cr}$
T	For $e^{in\pi/2}$ read $e^{-im\pi/2}$

There are a number of other typos that are either trivial or self-evident.

REFERENCES

[1]Ribner, H. S., "Convection of a Pattern of Vorticity Through a Shock Wave", NASA TN 2864, Jan. 1953; NACA Rep. 1164, 1954.

[2]Moore, F. K., "Unsteady Oblique Interaction of a Shock Wave with a Plane Disturbance", NACA TN 2879, 1953; NACA Rep. 1165, 1954.

[3]Kerrebrock, J. L., "The Interaction of Flow Discontinuities with Small Disturbances in a Compressible Fluid", Ph.D. Thesis, Calif. Inst. of Technology, 1956.

[4]Chang, C. T., "Interaction of a Plane Shock and Oblique Plane Disturbances with Special Reference to Entropy Waves", Journal of the Aeronautical Sciences, pp. 675-682, Sept. 1957.

[5]Ribner, H. S. and Tucker, M., "Spectrum of Turbulence in a Contracting Stream", NACA TN 2606, Jan. 1952.

[6]Ribner, H. S., "Shock-Turbulence Interaction and the Generation of Noise", NACA TN 3255, July 1954; NACA Rep. 1233, 1955.

[7]Batchelor, G. K., The Theory of Homogeneous Turbulence, Cambridge University Press, Cambridge, 1953, pp. 29 and 49.

[8]Moyal, J. E., "The Spectra of Turbulence in a Compressible Fluid; Eddy Turbulence and Random Noise", Proc. Cambridge Phil. Soc., 48, Pt. 2, April 1952, pp. 329-344.

[9]Grande, E. and Oates, G. C., "Unsteady Flow Generated by Shock-Turbulent Boundary Layer Interactions", AIAA Paper 73-168, 1973.

[10]Trolier, J. W. and Duffy, R. E., "Turbulence Measurements in Shock-Induced Flows", AIAA Journal, Vol. 23, No. 8, Aug. 1985, pp. 1172-1178.

[11]Anyiwo, J. C. and Bushnell, D. M., "Turbulence Amplification in Shock Wave Boundary Layer Interactions', AIAA Journal, Vol. 20, July 1982, pp. 893-899.

[12]Zang, T. A., Hussaini, M. Y. and Bushnell, D. M., "Numerical Computations of Turbulence Amplification in Shock-Wave Interactions", AIAA Journal, 22(1), Jan. 1984, pp. 13-21.

[13]Zang, T. A., Kopriva, D. H. and Hussaini, M. Y., "Pseudospectral Calculation of Shock-Turbulence Interactions", NASA Contractor Rep. 172133, Institute for Computer Applications in Science and Engineering (ICASE), NASA Langley Research Center, Hampton, Va., May 1983.

[14]Ram, G. S. and Ribner, H. S., "The Sound Generated by Interaction of a Single Vortex with a Shock Wave", Heat Transfer and Fluid Mechanics Institute, Stanford University, 1957, pp. 1-21; also Ribner, H. S., Univ. of Toronto Institute for Aerospace Studies, UTIA Rep. 61, 1959.

[15]Ribner, H. S., "Cylindrical Sound Wave Generated by Shock-Vortex Interaction", AIAA Journal, 23 (11), pp. 1708-1715, Nov. 1985.

[16]Hollingsworth, M. A. and Richards, E. J., "On the Sound Generated by the Interaction of a Vortex and a Shock Wave" (British) Aeronautical Research Council, Rep. 18 257, FM 2371, Feb. 1956.

[17]Dosanjh, D. S. and Weeks, T. M., "Interaction of a Starting Vortex as Well as a Vortex Street with a Travelling Shock Wave", AIAA Journal, 3(2), pp. 216-223, Feb. 1965.

[18]Pao, S. P. and Seiner, J. M., "Shock Associated Noise in Supersonic Jets", AIAA Journal, 21(5), pp. 687-693, May 1983.

[19]Tatarski, V. I., Wave Propagation in a Turbulent Medium, New York: McGraw-Hill, 1961, p. 5.

[20]Etkin, Bernard, Dynamics of Atmospheric Flight, John Wiley & Sons, 1972, p. 539.

[21]Ribner, H. S., "Acoustic Energy Flux from Shock-Turbulence Interaction", J. fluid Mech., 35, Part 2, pp. 299-310, 1969.

[22]Blokhintsev, D. I., Acoustics of a Nonhomogeneous Moving Medium, NACA TM 1399, Feb. 1956 (translation of 1946 Russian paper).

[23]Batchelor, G. K., "The Theory of Axisymmetric Turbulence", Proc. Roy. Soc. A, 186, pp. 480-502, 1946.

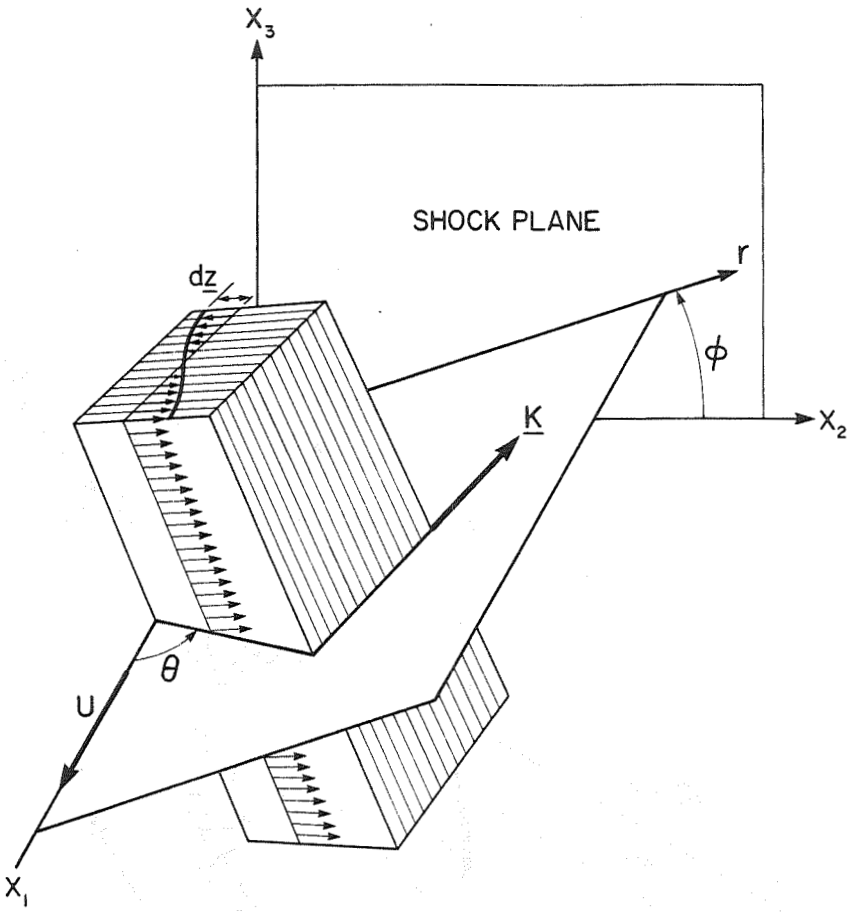

FIG. 1 PERSPECTIVE VIEW OF SHEAR WAVE (3D SPECTRAL COMPONENT OF TURBULENCE) IN RELATION TO REFERENCE FRAME. NOTE THAT dZ IS NOT IN GENERAL IN THE PLANE OF K AND U.

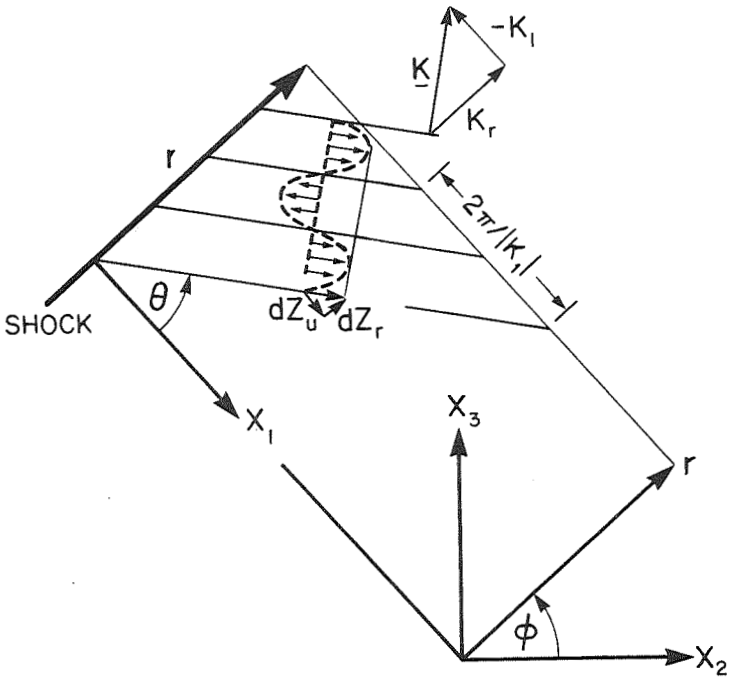

FIG. 2 PROJECTIVE VIEW OF SHEAR WAVE IN RELATION TO REFERENCE FRAME.

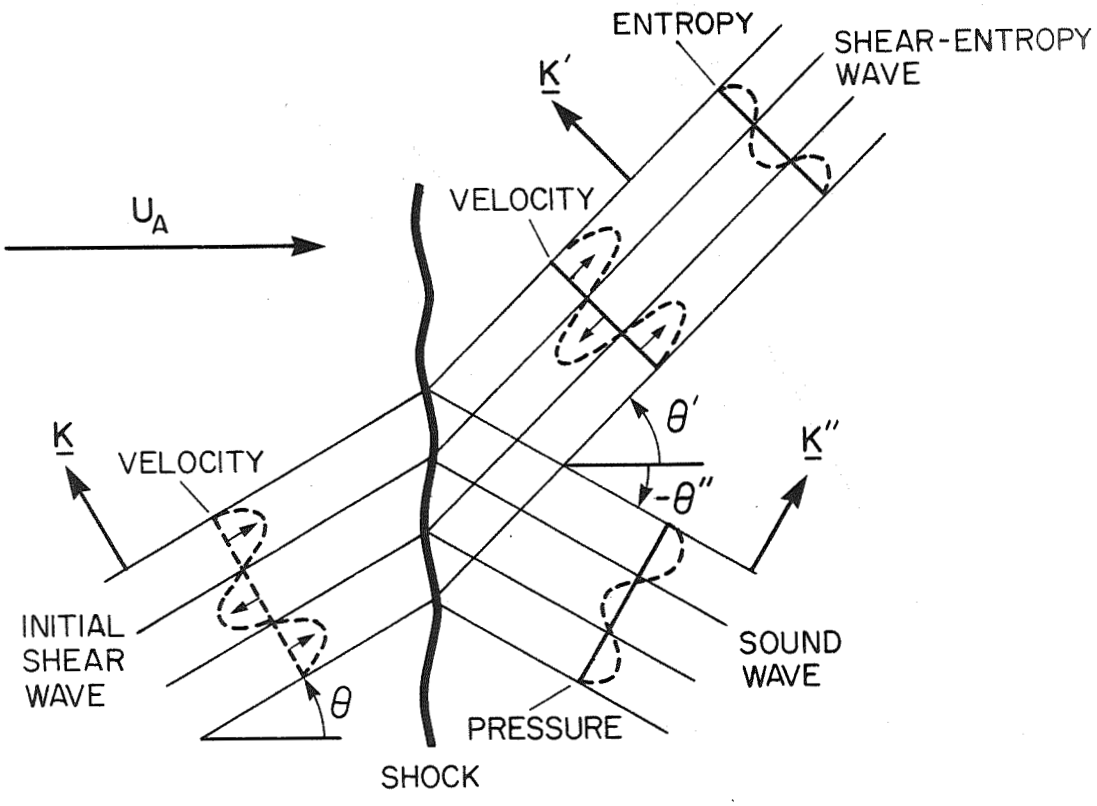

FIG. 3 INTERACTION OF SHEAR WAVE WITH SHOCK: VIEW IN X_1, r-PLANE.

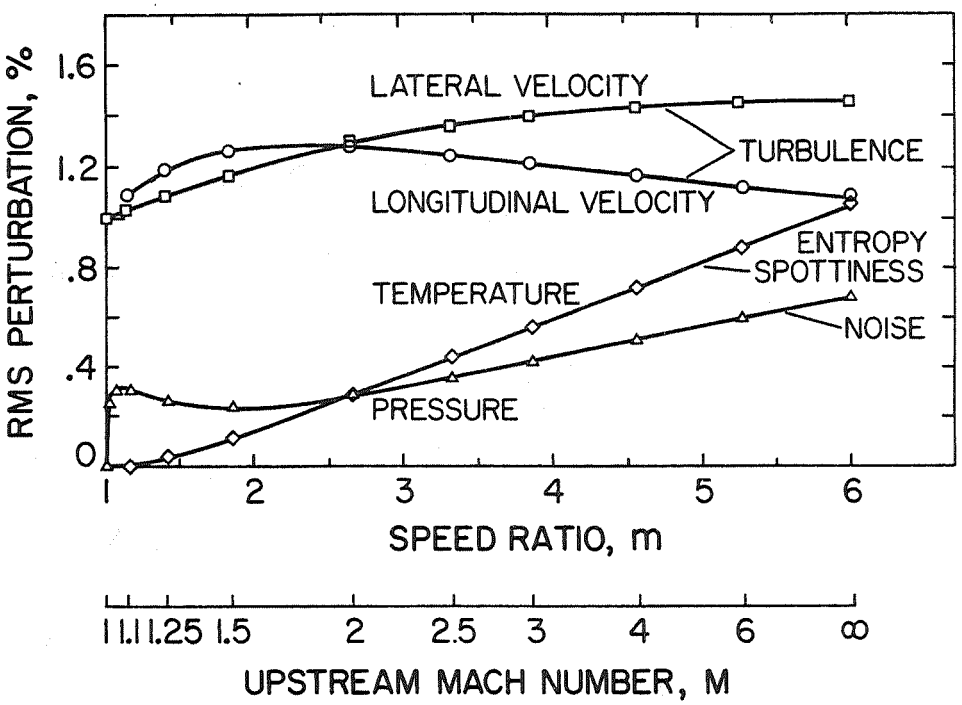

FIG. 4 AMPLIFIED TURBULENCE AND OTHER DISTURBANCES PRODUCED DOWNSTREAM OF SHOCK BY INTERACTION WITH ISOTROPIC TURBULENCE. PRESHOCK TURBULENCE INTENSITY 1%. RMS VELOCITIES IN PERCENT OF INITIAL STREAM VELOCITY; RMS TEMPERATURE AND PRESSURE (NOISE) IN PERCENT OF AMBIENT.

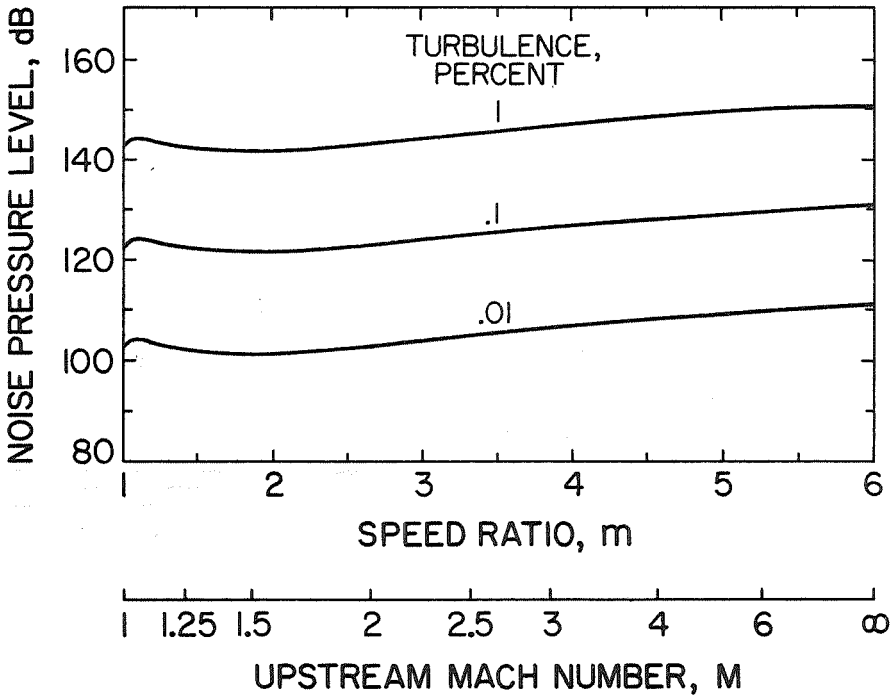

FIG. 5 NOISE GENERATED BY SHOCK-TURBULENCE INTERACTION (ISOTROPIC TURBULENCE) ON A DECIBEL SCALE. POSTSHOCK AMBIENT PRESSURE, 1 ATM.

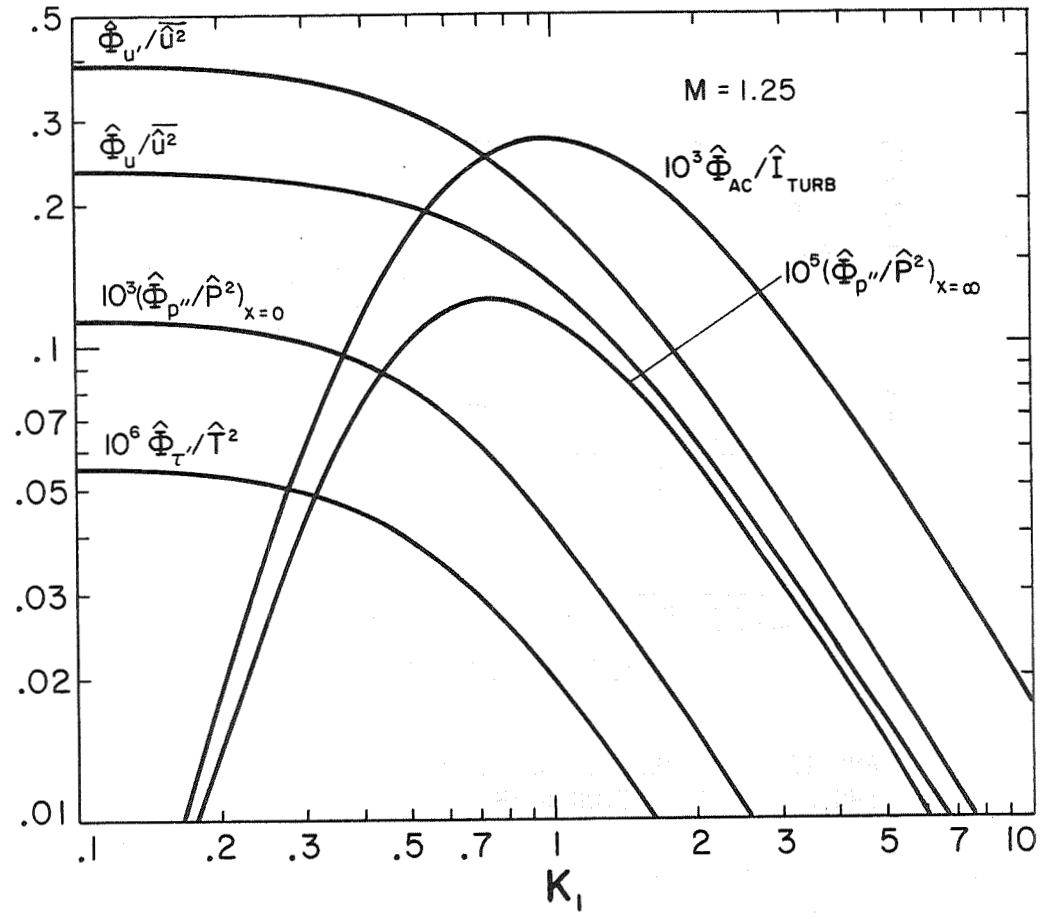

FIG. 6 NORMALIZED 1D POWER SPECTRA OF THE SHOCK-INTERACTION PRODUCTS WHOSE RMS VALUES ARE GIVEN IN FIG. 4 (EXCEPT $\Phi_{v'}/\overline{u^2}$) PLUS TWO OTHERS (SEE TEXT). MACH NUMBER M = 1.25 ONLY.

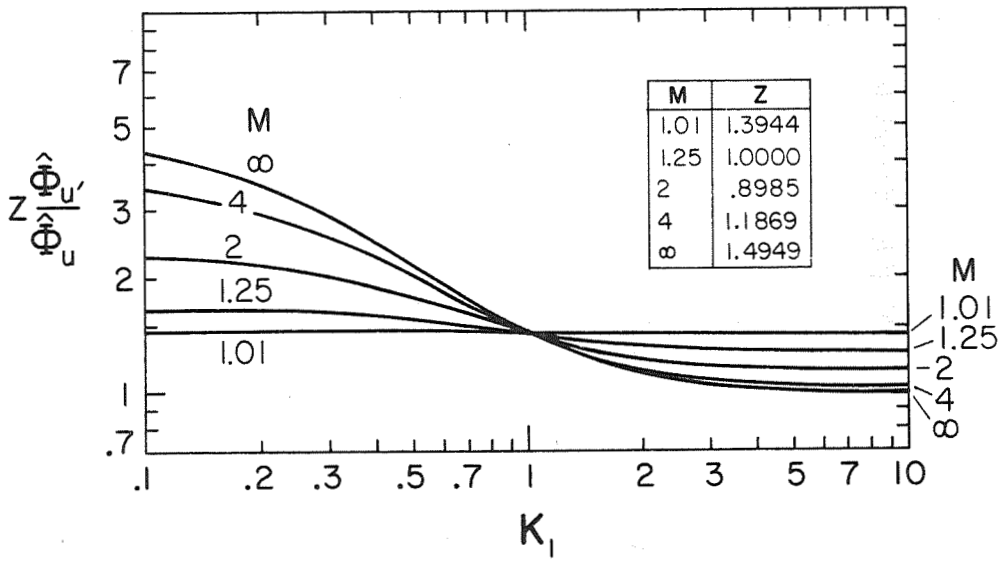

M	Z
1.01	1.3944
1.25	1.0000
2	.8985
4	1.1869
∞	1.4949

FIG. 7 RATIO OF 1D SPECTRA FOR ISOTROPIC PRESHOCK TURBULENCE: POSTSHOCK LONGITUDINAL COMPONENT/PRESHOCK LONGITUDINAL COMPONENT.

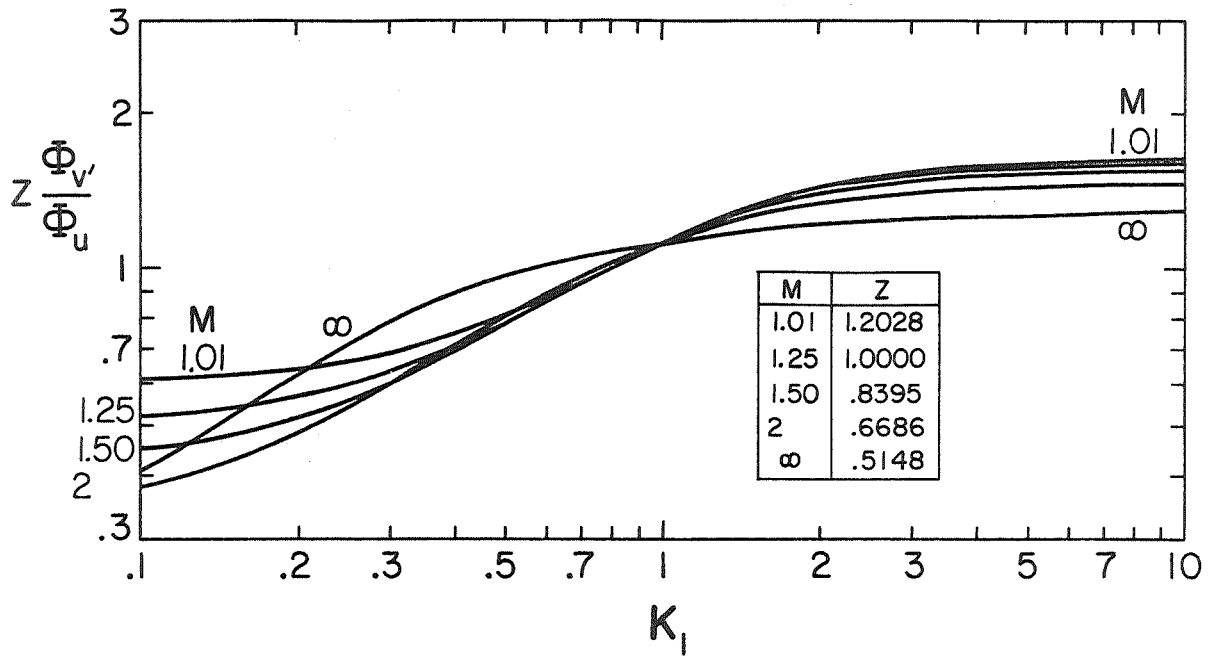

FIG. 8 RATIO OF 1D SPECTRA FOR ISOTROPIC PRESHOCK TURBULENCE: POSTSHOCK LATERAL COMPONENT/PRESHOCK LONGITUDINAL COMPONENT.

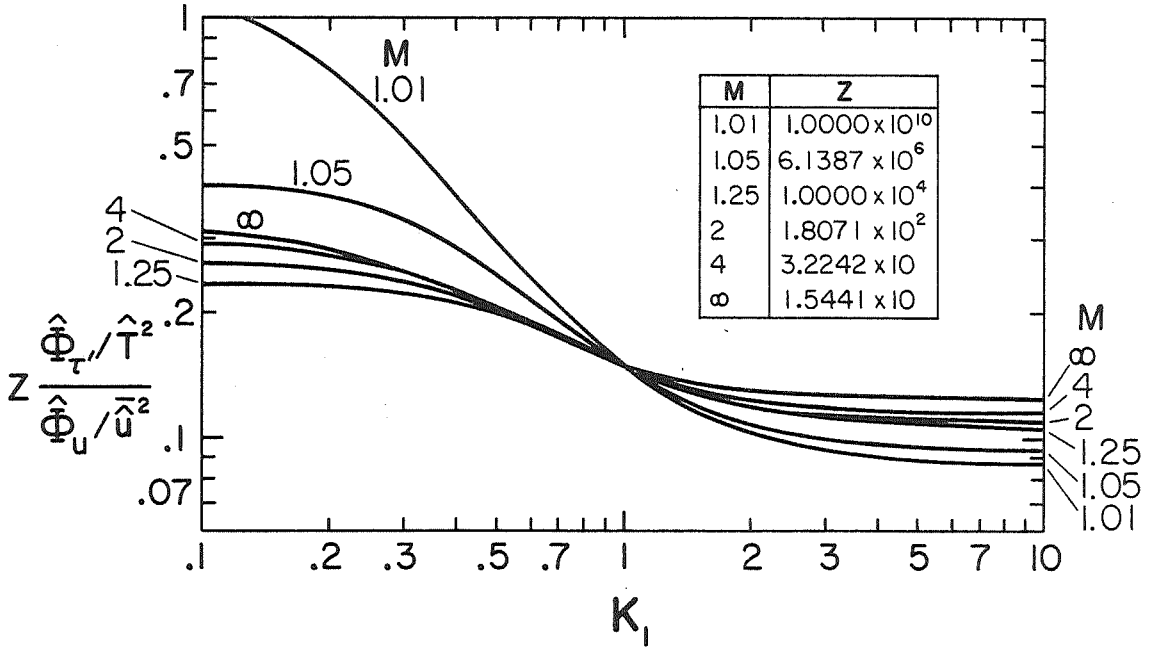

FIG. 9 RATIO OF 1D SPECTRA FOR ISOTROPIC PRESHOCK TURBULENCE: POSTSHOCK TEMPERATURE FLUCTUATION/PRESHOCK LONGITUDINAL COMPONENT OF TURBULENCE (BOTH NORMALIZED).

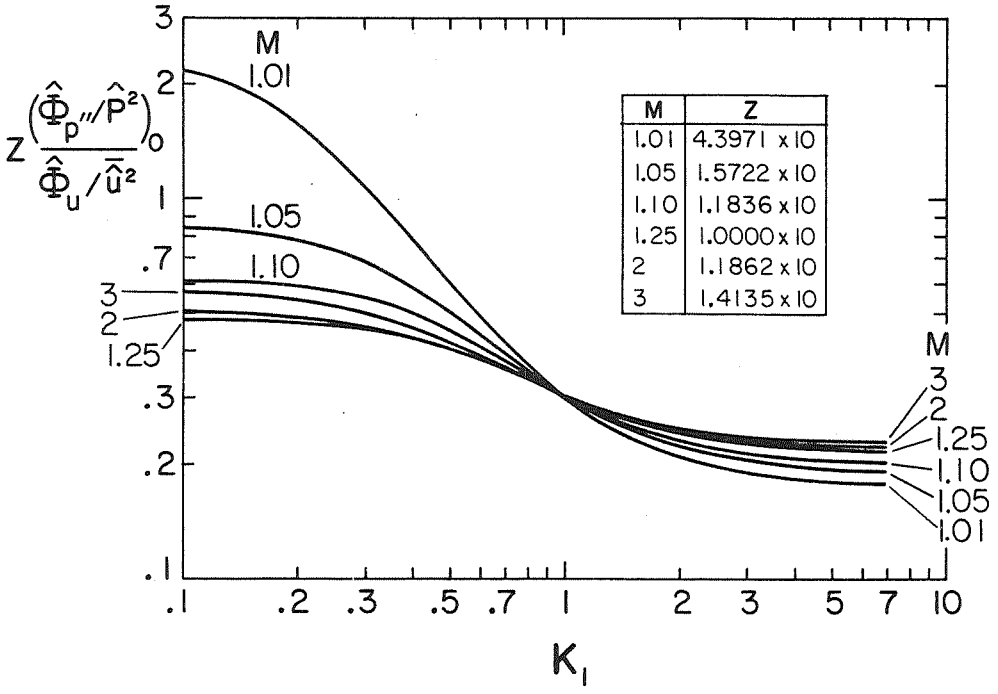

FIG. 10 RATIO OF 1D SPECTRA FOR ISOTROPIC PRESHOCK TURBULENCE: "NEAR FIELD" NOISE (X = 0)/PRESHOCK LONGITUDINAL COMPONENT OF TURBULENCE (BOTH NORMALIZED).

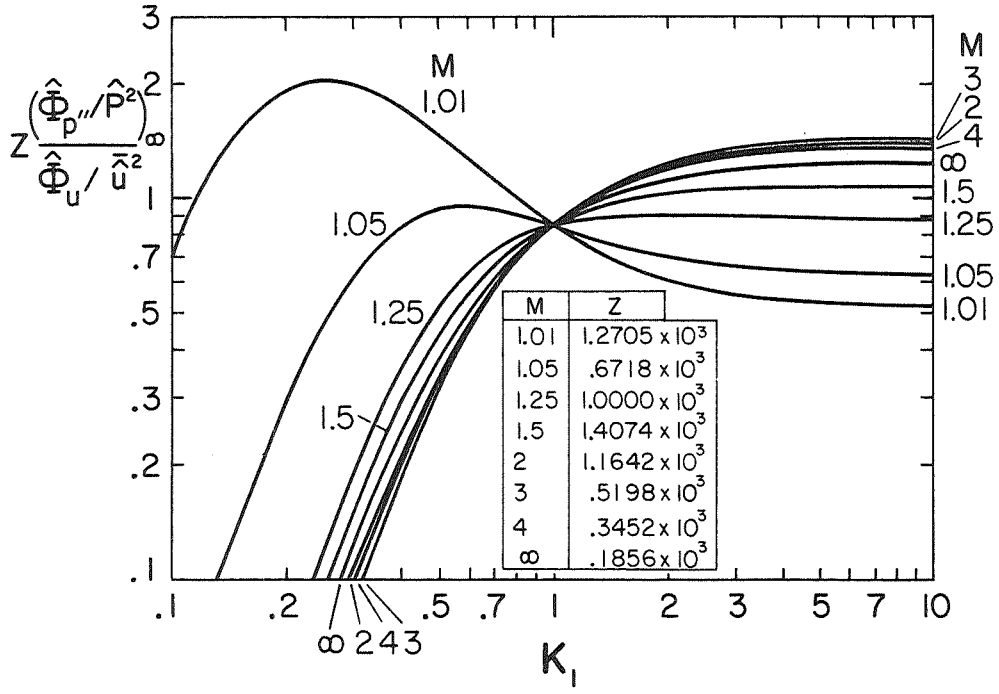

FIG. 11 RATIO OF 1D SPECTRA FOR ISOTROPIC PRESHOCK TURBULENCE: POSTSHOCK "FAR FIELD" NOISE (X = ∞)/PRESHOCK LONGTUDINAL COMPONENT OF TURBULENCE (BOTH NORMALIZED).

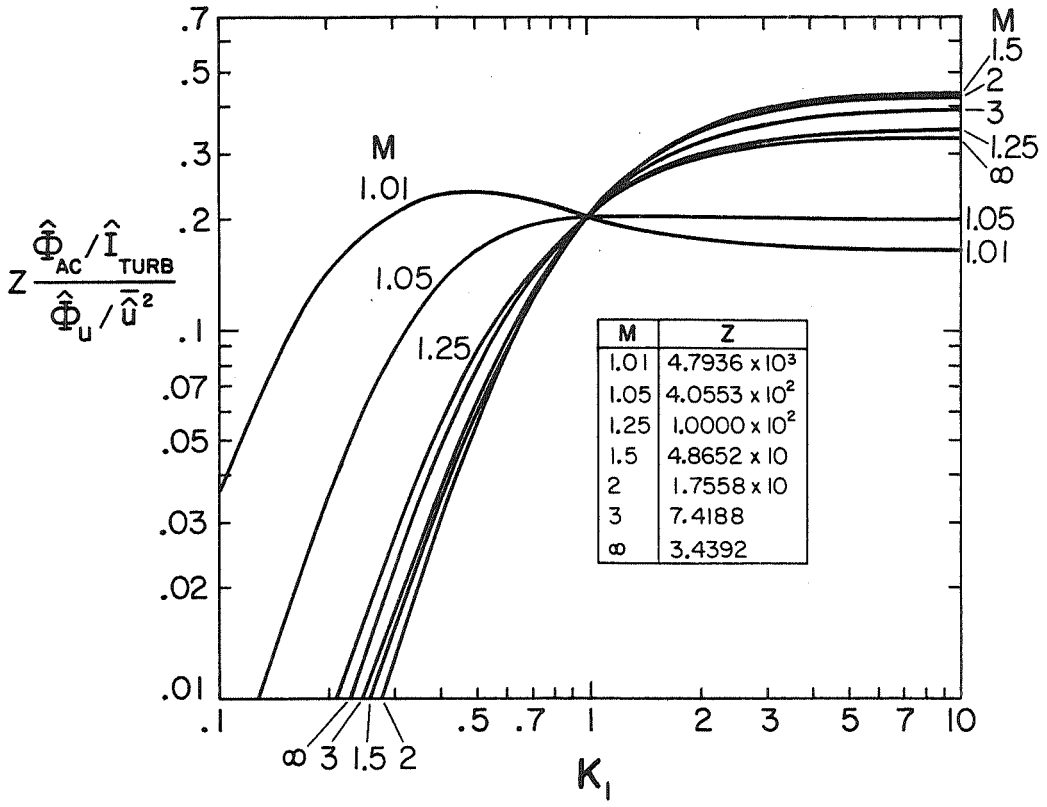

FIG. 12 RATIO OF 1D SPECTRA FOR ISOTROPIC PRESHOCK TURBULENCE: POSTSHOCK ACOUSTIC ENERGY FLUX (NORMALIZED BY PRESHOCK TURBULENCE ENERGY FLUX)/PRESHOCK LONGITUDINAL COMPONENT OF TURBULENCE (NORMALIZED BY MEAN SUARE VALUE).

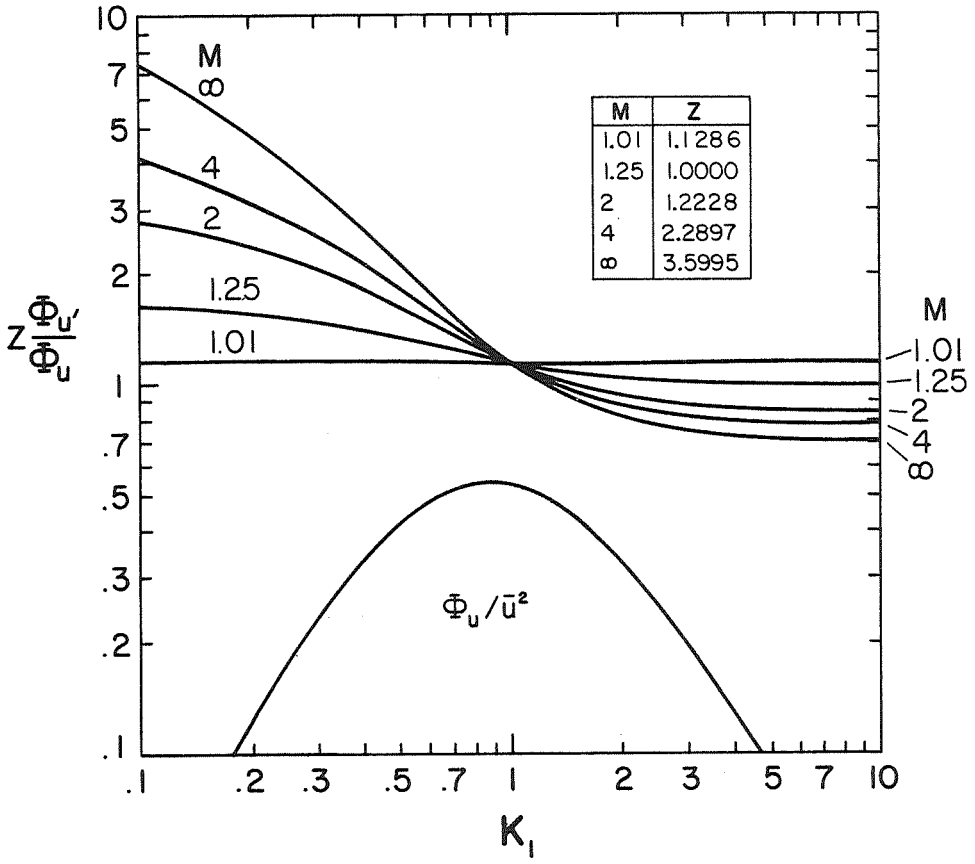

FIG. 13 RATIO OF 1D SPECTRA FOR AXISYMMETRIC PRESHOCK TURBULENCE: POSTSHOCK LONGITUDINAL COMPONENT/PRESHOCK LONGITUDINAL COMPONENT.

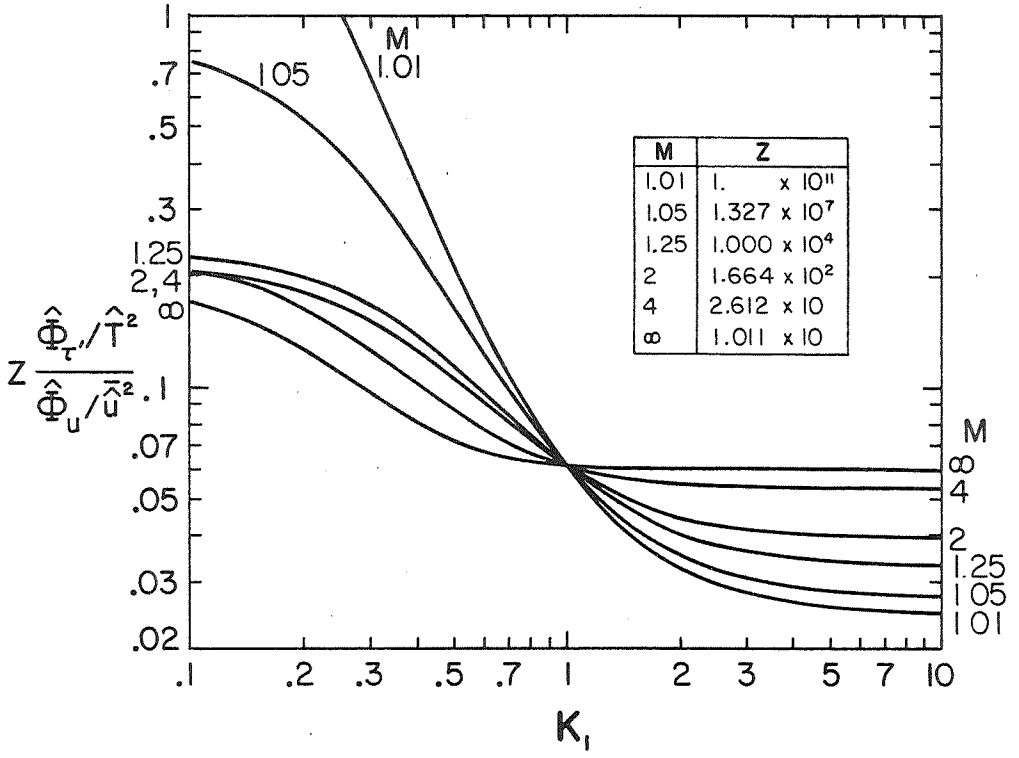

FIG. 14 RATIO OF 1D SPECTRA FOR AXISYMMETRIC PRESHOCK TURBULENCE: POSTSHOCK TEMPERATURE FLUCTUATION/PRESHOCK LONGITUDINAL COMPONENT OF TURBULENCE (BOTH NORMALIZED).

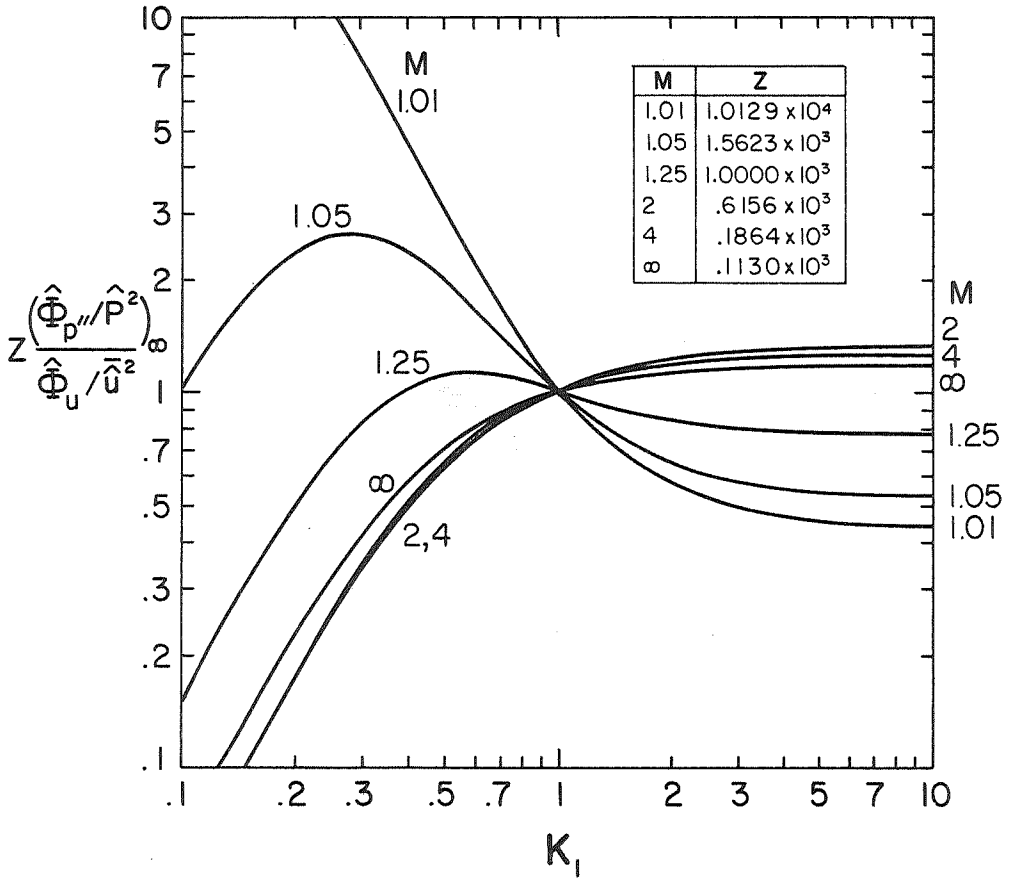

FIG. 15 RATIO OF 1D SPECTRA FOR AXISYMMETRIC PRESHOCK TURBULENCE: POSTSHOCK "FAR FIELD" NOISE (X = ∞)/PRESHOCK LONGITUDINAL COMPONENT OF TURBULENCE (BOTH NORMALIZED).